International Journal of Automation and Computing

17(2), April 2020, 222-232
DOI: 10.1007/s11633-019-1188-5

Spectral-spatial Classification of Hyperspectral Images Using Signal Subspace Identification and Edge-preserving Filter

Negin Alborzi[1] Fereshteh Poorahangaryan[2] Homayoun Beheshti[1]

[1] Department of Computer Engineering, Faculty of Electrical and Computer Engineering, Ayandegan Institute of Higher Education in Tonekabon, Mazandaran 4681853617, Iran

[2] Department of Electrical Engineering, Faculty of Electrical and Computer Engineering, Ayandegan Institute of Higher Education in Tonekabon, Mazandaran 4681853617, Iran

Abstract: Hyperspectral images in remote sensing include hundreds of spectral bands that provide valuable information for accurately identify objects. In this paper, a new method of classifying hyperspectral images using spectral spatial information has been presented. Here, using the hyperspectral signal subspace identification (HYSIME) method which estimates the signal and noise correlation matrix and selects a subset of eigenvalues for the best representation of the signal subspace in order to minimize the mean square error, subsets from the main sample space have been extracted. After subspace extraction with the help of the HYSIME method, the edge-preserving filtering (EPF), and classification of the hyperspectral subspace using a support vector machine (SVM), results were then merged into the decision-making level using majority rule to create the spectral-spatial classifier. The simulation results showed that the spectral-spatial classifier presented leads to significant improvement in the accuracy and validity of the classification of Indiana, Pavia and Salinas hyperspectral images, such that it can classify these images with 98.79%, 98.88% and 97.31% accuracy, respectively.

Keywords: Hyperspectral image, remote sensing, the hyperspectral signal subspace identification (HYSIME), edge-preserving filter, classification, support vector machine.

1 Introduction

Remote sensing technology is a data collection method in which contact with the measured objects is minimal. Collecting electromagnetic waves for measurement and recording is among the responsibilities of the sensors[1]. Hyperspectral imaging systems include several hundred spectral bands and possess high spectral accuracy. Based on the nature of the datum it carries, every pixel of the image has a unique spectral graph, called its spectral signature[2]. One of the most important applications of remote sensing science is allocating a class to every pixel, called classification[2]. Nowadays, most research in the field of remote sensing technology focuses on hyperspectral images[3]. The spectral-spatial classification of hyperspectral images has faced such challenges as the complexity of the area under study, data selection, image and algorithm processing. There are various approaches toward creating a classifier with reasonable accuracy. Much of the mentioned research uses techniques which allocate a class to each pixel solely based on its spectral value without considering the information contained within the neighboring pixels[4]. Bayesian networks[4], decision trees[4], neural networks[5], kernel-based techniques[6], and support vector machine (SVM)[7] have been proposed for this purpose. Spectral-spatial classification of hyperspectral images distinguishes different classes using spatial neighborhood dependence of the pixels and is the best method for recognizing patterns with high accuracy in order to improve image classification. Research has shown that spectral-spatial filters have adequate performance in the spectral-spatial classification of hyperspectral images. An important class of these filters are edge-preserving filters. Recently, edge-preserving filtering[8–12] has become an active research topic in the field of remote sensing and has found applications in image segmentation, classification, dimensionality reduction, feature extraction, and noise cancellation[13–16]. The dimensionality reduction method tries to reduce the number of features of each subject and to fully separate the classes in the hyperspectral image. The feature extraction method reduces data dimensions by selecting a subset of the initial features[17]. Image feature extraction is an important operation in remote sens-

Research Article
Manuscript received February 14, 2019; accepted June 5, 2019; published online September 25, 2019
Recommended by Associate Editor De Xu

ing and has been used for content-based image comparison and for image analysis. Feature extraction has been employed in the last two decades in diverse applications such as medicine, industry, machine vision, and control. In machine vision, image processing, and remote sensing, using various mathematical operations like edge detection using gradients and appropriate filtering, the image features have been extracted[18]. In recent years, various algorithms have been proposed for image feature extraction. The existing methods extract all the characteristics of features that are sensitive to noise and dependent on the complexities of image patterns[18]. Zhang et al.[19] introduce a new index called the mutual information (MI) and applied it for determination of the specific bands of the satellite images.

In spite of limitations in spatial data and the complexity of feature merging, the spectral data has not been eliminated after filtering. To solve this problem, a method of image feature extraction using a propagated filter (PF) has been presented (PCA-PF-SVM)[20]. After dimensionality reduction using PCA and extracting the image features, the PF has been applied to the image, and it has been classified using the SVM classifier[20]. Combining different areas in an image is another challenge for the existing filters when they process the image for noise cancellation. The propagated filter cancels noise and smooths the image using the characteristics of bilateral filters and, hence, has a smaller computational burden relative to other filters[21]. Results show that this method effectively extracts the spectral-spatial features of hyperspectral images and considerably improves classification accuracy[21].

Kang et al.[8], for first time, introduce a new structure based on edge-preserving filtering (EPF) for the spectral-spatial classification. Their structure includes the following steps:

First, the hyperspectral image is classified using pixel classification, i.e., a support vector machine classifier. Then, the resulting classified map is presented as probabilistic maps in different classes, and edge-preserving filtering is applied to each of the probabilistic maps in the classes given the first main component or the first three main components of the hyperspectral image presented as the reference grey or color image. Finally, the maximum value on the filtered probabilities is chosen for the final classification. Experimental results show that edge-preserving filtering can significantly improve classification accuracy, and therefore can be used in real-world applications[8].

Xia et al.[11] first, used a popular strategy based on the random subspace (RS) for extraction of K band randomly. Then, independent component analysis (ICA) is used to extract the independent spectral components, and EPF is used to generate spatial-spectral features. Finally, using random classifications, random forest, and random rotation, classification is performed[11].

Note that efficient band selection from hyperspectral images and its role in classification accuracy is one of the vital challenges in research. On the other hand, in preprocessing stage, the selection of suitable filters is a sensitive task; i.e., if the mentioned filter is not so efficient some information may be missed. Moreover, the random selection of subspace may be eliminated by the important subspaces that have more information.

The contributions of this paper are threefold.

1) We present a new strategy without using any of the randomness extraction of subspaces. The use of the hyperspectral signal subspace identification (HYSIME) technology for the subspace selection.

2) We propose a new structure from the combination of the HYSIME method, edge-preserving filtering, and the SVM classifier for the spectral-spatial classification of hyperspectral images.

To carry out this task, the hyperspectral subspaces are extracted from the image, and edge-preserving filtering is applied to the individual subspaces. The results of the classification obtained from the presented method are merged into the decision-making level using majority rule to create the spectral-spatial classification. The proposed method is capable of improving classification accuracy and performance, reduce complexity, reduce stored data volume, cancel small noise, maintain the original structure of the image, identify subspaces, and automatically reduce dimensions. Hyperspectral signal identification with minimum error starts with signal evaluation and noise correlation matrices, using multiple regression. Then a subset of inputs of the correlation matrix of the signal is used to represent the subspace of the signal. This subspace is obtained by minimizing the total power of the prediction error with noise power, which decreases and increases the function of the subspace function, respectively. Therefore, if dimensions are ignored under the space, the power of noise is dominant, while if the dimensions are below space, the error of the prediction error is dominant. The overall layout of the computational performance is uncontrolled and completely automated, which means that no parameters are set.

In Section 2, the determination of hyperspectral signal subspaces using HYSIME has been described. Section 3 has explained the edge-preserving filter. The proposed method and its experimental results have been explained in Section 4. The final part involves results and discussion about the proposed method.

2 Signal subspace estimation using HYSIME

The hyperspectral subspace method was presented in [22, 23] in recent decades. Every pixel of a hyperspectral image may be represented by a spectral vector where each of the spectral bands represents an axis in space.

The number of pure members present in an area is far fewer than the number of bands covering that area. For this reason, an important issue for high-dimensional data is determining their real number of dimensions. Identifying such a subspace enables one to display the spectral vectors in a subspace with fewer dimensions. This process is known as data dimensionality reduction, and it leads to a lower computational burden and stored data volume[23]. Dimensionality reduction is one of the most important preprocessing steps in hyperspectral processing. High-dimensional data possesses two important characteristics: first, they can be projected onto subspaces with fewer dimensions without any data loss, and second, the number of training samples increases with the number of data dimensions. Therefore, it is necessary to project high-dimensional data onto low-dimension subspaces without loss of data[23]. HYSIME is one of the modern methods of estimating the signal subspace in the hyperspectral images, and it is based on minimizing the mean square error. In this method, the dimensionality of the hyperspectral space is determined by minimizing the sum of the powers of the image error and noise error terms. Here, the noise and signal correlation matrix is first estimated using multiple linear regression then, the eigenvectors of the signal correlation matrix are used to generate a series of nested subspaces[23]. After that, the signal subspace is determined by minimizing the sum of the powers of the image error and the noise error terms which are, respectively, descending and ascending functions of the subspace dimensionality. Hence, if the subspace dimensionality is higher than the true value, the term pertaining to the power of the noise error will prevail, whereas if the subspace dimensionality is lower than the true value, the term pertaining to the power of the image error will prevail[23]. In the first stage, a number of orthogonal directions that create an undetermined subspace out of the signal subspace are determined. This undetermined subspace is determined by searching for the minimum mean square error between the min signal X and the input data, i.e., the observed spectral vector $r = X + n$. The correlation matrix is denoted by R_x[23].

$$Rx = \frac{[X_1, X_2, \cdots, X_n]\,[X_1, X_2, \cdots, X_n]^{\mathrm{T}}}{N} \tag{1}$$

where X is the signal estimated after subtracting the noise estimated in the previous step from the main hyperspectral data. The eigenvalues of the hyperspectral correlation matrix have been sorted in descending order. Now, the R^L space may be decomposed into two orthogonal subspaces: the first-order moment and the second-order moment obtained using (2) (k is the dimensionality of the subspace).

$$E\,(K_k|X) = U_k E(Y|X) = U_k E(Y + n|X) = U_k X = X_k. \tag{2}$$

The mean square error between X and X_k equals:

$$\begin{aligned}\mathrm{MSE}(K|X) = E\left[(X - X_k)^{\mathrm{T}}\,(X - X_k)\,|X\right] = \\ E\left[(X - X_k - U_k n)\,\mathrm{T}\,(X - X_k - U_k n|X\right] = \\ (X - X_k)^{\mathrm{T}}\,(X - X_k) + \left(U_k R_n U_k^{\mathrm{T}}\right)^{\mathrm{T}}.\end{aligned} \tag{3}$$

Finally, an estimate of the hyperspectral subspace is obtained by minimizing the mean square error using the above relationship. The correlation matrix $R_Y = \dfrac{YY^{\mathrm{T}}}{N}$ has been replaced with that of the samples [23].

$$(k, {}_{\pi\pi}) = \arg\,\min\left\{(U_{k\perp\perp} R_Y)^{\mathrm{T}} + 2(U_k R_n)^{\mathrm{T}}\right\}. \tag{4}$$

3 Edge-preserving filtering

The dge-preserving filter is an image processing technique the objective of which is reducing spatial variety. It smooths textures and preserves edges. For high-resolution hyperspectral images, neighboring pixels usually have strong connections. Using the edge-preserving filter causes neighboring pixels on the same side of an edge to possess similar features which helps improve the performance of the classification[24]. Using edge-preserving filters in optimizing subsets has two advantages: first, noise subsets which appear as scattered points can be effectively smoothed, and second, restored subsets are always level with the boundaries of the actual object[8]. These advantages show that the spatial information of the reference image have been well taken advantage of in the filtration process[8, 24]. The edge-preserving filter based on the Gaussian filter is used. The spatial and range distances are defined using two Gaussian decreasing functions, i.e., $G_{\delta s}\left(\|\| i-j \|\|\right) = \exp\left(\dfrac{-\left(\|\| i-j \|\|\right)}{\delta_s^2}\right)$ and $G_{\delta r}\left(\|I_i - I_j\|\right) = \exp\left(\dfrac{-|I_i - I_j|^2}{\delta_r^2}\right)$[24]. In the edge-preserving filter, spatial distances are defined using two G functions, where O_i is the filter output, P_j the input image, I the reference image (It is the same variable as that for the reference image). i and j are the pixels. Those neighboring pixels that share similar intensity and color tend to have similar outputs and are defined as follows[8]. In the edge-preserving filter, spatial distances are defined using two G functions, where O_i is the filter output, P the input image, I the reference image, and I and j are the pixels. K_b is a normalizing term of the edge-preserving filter, δs controls the size of the local window used to filter a pixel, and δr defines how much the weight of a pixel decreases because of the intensity difference between the reference pixels[8]. Those neighboring pixels that share similar intensity and color tend to have similar outputs and are defined as follows:

$$O_i = \frac{1}{K_i^b} \sum_{j \in \omega i} \sum_{j \in \omega i} G_{\delta s}\left(\| i - j \|\right) G_{\delta r}\left(|I_i - I_j|\right) P_j. \quad (5)$$

4 Proposed method

Fig. 1 displays the structure of the proposed method. This method has four steps: 1) estimating the hyperspectral signal subspace explained in Section 2, 2) edge-preserving filtering of the subspaces, 3) classifying the filtered subspaces, and 4) merging the classification results using majority rule.

As explained in the description of the HYSIME method in Section 2, after estimating the correlation matrix of the sample signal, a set is introduced, an unknown subset of which forms the hyperspectral subspace. Where the sum of the powers of the image error and the noise error is minimized, i.e., the optimal solution, the dimensions of the hyperspectral subspace are calculated[8]. In the next stage, edge-preserving filtering has been applied to all subspaces. When the size of the filter and the opaqueness of the image increase, the filtration outputs are smoother, and the neighboring input pixels of similar intensities in the reference image tend more to assimilate to the filtration outputs. By applying edge-preserving filtration to the hyperspectral subspaces and considering spatial data, the reference image is obtained. In the filtration of the subspaces, spatial data are not initially taken into account. Therefore, the subspaces have noise and are not level with the boundaries of the actual object. To solve this problem, the extracted subspaces are optimized through edge-preserving filtration[8]. Hence, this step faces two challenges: 1) the choice of the edge-preserving filter, and 2) the reference image[14]. Optimizing subspaces using edge-preserving filtration has two main advantages: 1) noise subsets which appear as scattered points can be effectively smoothed, and 2) restored subsets are always level with the boundaries of the actual object. These points indicate that the spatial data have been used well in the edge-preserving filtration process[8]. After this stage, the SVM classification is applied to the filtered subspaces. Among the reasons for choosing this classifier are the facts that it is one of the mostly used pixel classifiers, has adequate performance in spectral-spatial classification applications, and is resistant against noise and the Hughes phenomenon. Furthermore, the information fusion from the point of view of features and decision making have been established in [11, 25]. The results obtained from the classifier are merged into the decision-making level using majority rule, and finally the classification map is generated. The merging of the classification results leads to an improved classification, such that novel results with more comprehensive data may be attained. The merging process is one which does cause loss of spectral data and which fully preserves spectral features and adds spatial features to the hyperspectral images[26].

4.1 Hyperspectral data sets

The proposed method is performed on three hyperspectral data sets, i.e., the Indian Pines image, the University of Pavia, and the Salinas image. The pictures have the following characteristics:

Indian Pines: The first hyperspectral image. The Indian Pines image capturing the agricultural Indian Pine test site of north-western Indiana was acquired by the airborne visible/infrared imaging spectrometer (AVIRIS) sensor. The image has 220 bands of size 145×145 with a spatial resolution of 20 m per pixel and a spectral coverage ranging from 0.4 µm to 2.5 µm[8]. The reason for choosing this image, similar spectral signatures of different classes and the complexity is in the classification. After removing bands of noise and water absorption, experiments are performed on the remaining 186 bands. Fig. 2 (a) shows the corresponding ground truth data of the Indian Pines image.

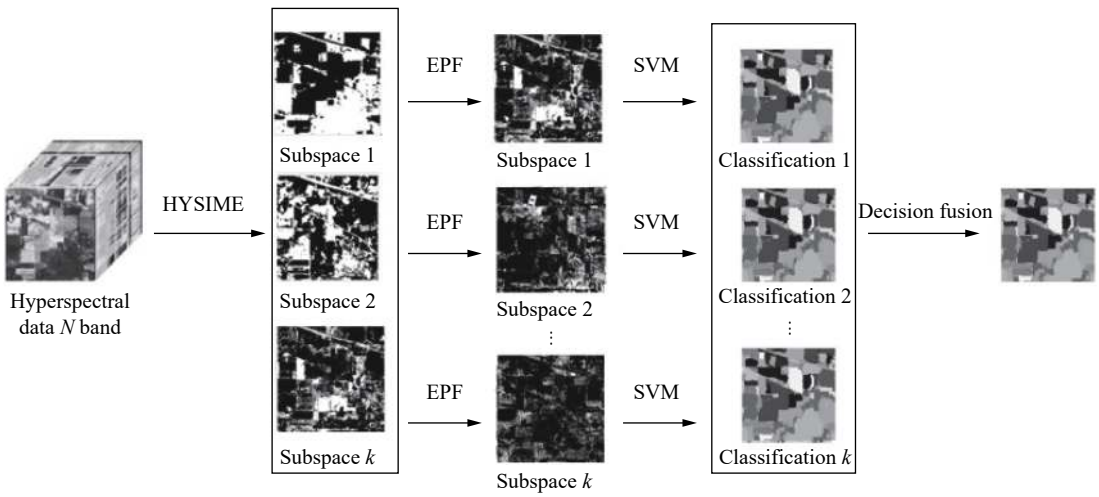

Fig. 1 Schematic of the proposed, spectral-spatial classification method

University of Pavia: The University of Pavia image capturing an urban area surrounding the University of Pavia was recorded by the ROSIS-03 satellite sensor. The image has 115 bands of size 610×340 with a spatial resolution of 1.3 m per pixel and a spectral coverage ranging from 0.43 μm to 0.86 μm (12 most noisy channels were removed before experiments). Nine classes of interest are considered for this image[8]. Fig. 3 (a) shows the reference images of the University of Pavia dataset.

Salinas: The Salinas image was captured by the AVIRIS sensor over Salinas Valley, CA, USA, and with a spatial resolution of 3.7 m per pixel. The image has 224 bands of size 512×217. As with the Indian Pines and University of Pavia scenes, 20 water absorption bands were discarded[8]. Fig. 4 (a) shows the corresponding ground truth data of the Salinas image.

4.2 Quality indexes

In order to evaluate the performance of the proposed method, three quality indicators were used, namely, overall accuracy (OA), average accuracy (AA) and kappa coefficient. OA is the percentage of pixels which are properly categorized. AA is the average percentage of pixels for each class. The kappa coefficient corrects the correct percentage of classified pixels.

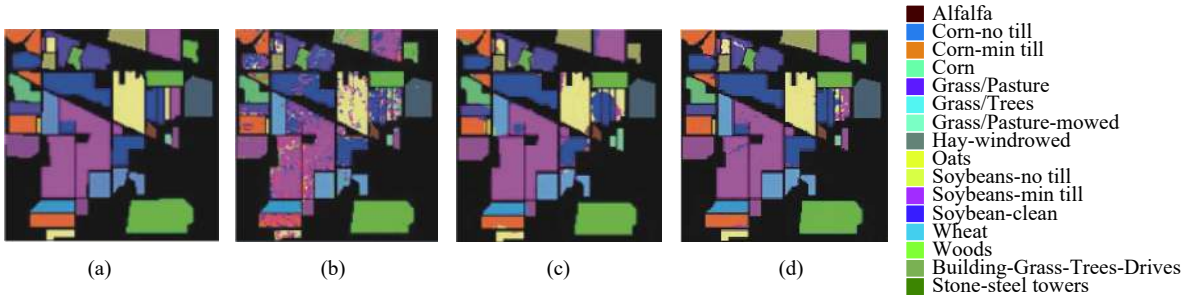

Fig. 2 Indian Pine image: (a) Ground truth data; (b) SVM method OA=79.53%; (c) RS-EPF-SVM method OA= 93.43%; (d) HYSIME-EPF-SVM Method OA=98.79%.

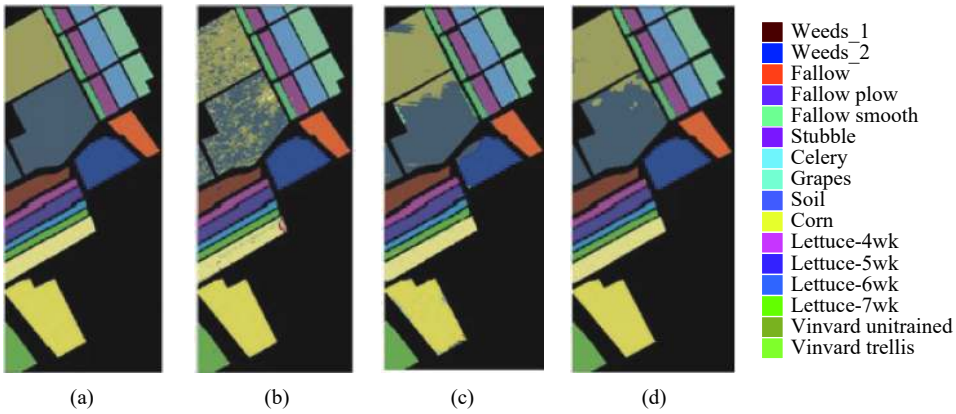

Fig. 3 Salinas image: (a) Ground truth data; (b) SVM method OA=89.21%; (c) RS-EPF-SVM method OA= 94.65%; (d) HYSIME-EPF-SVM method OA=97.31%.

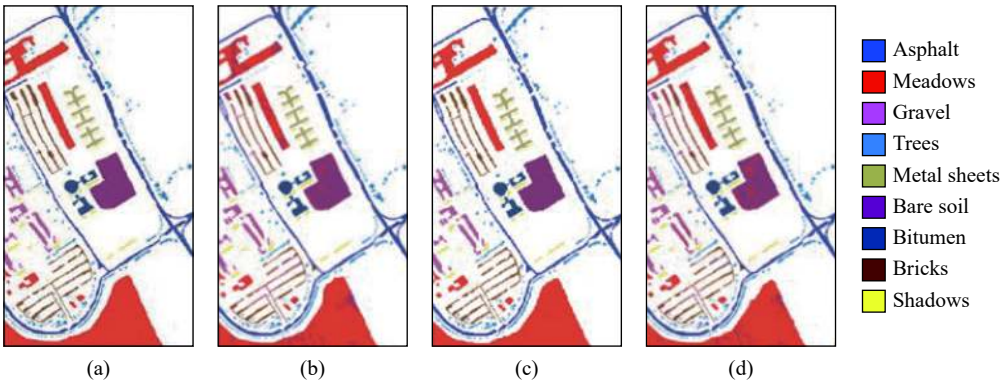

Fig. 4 University of Pavia image: (a) Ground truth data; (b) SVM method OA=90.57%; (c) RS-EPF-SVM method OA= 95.83%; (d) HYSIME-EPF-SVM method OA=97.31%.

4.3 Implementation results

The implementation has been conducted in Matlab software (a Laptop with 2.50GHz, 2CPU and 4-GB memory). Tables 1–3 show the hyperspectral subspace estimation using the HYSIME method as a function of the number of pure members (P), SNR, and the noise shape (white noise and Gaussian noise) in various on three hyperspectral data Indian Pines, Salinas and University of Pavia. For higher signal-to-noise ratio (SNR), better estimates of the pure members are obtained for white noise and Gaussian noise. Tables 1 and 2 are the results of hyperspectral subspace estimation it has been shown to Indian pines and Salinas with $P = 15$, SNR $= 50$ dB and $\eta = \frac{1}{18}$, $\eta = 0$ as an optimal solution. The minimum mean square error for these values is $K = 15$ which is equal to the number of pure members. So the value is $K = 15$ and 15 subspaces hyperspectral be extracted from these images. Also, in Table 3, the results of hyperspectral subspace estimation has been shown to University of Pavia with $P = 8$, SNR $= 50$ dB. Figs. 5 and 6, displays an assessment of the mean square error for the HYSIME algorithm in Indiana Pines and Salinas as a function of the subspace dimensionality with $P = 15$ and SNR $= 50$ dB, for $\eta = 0$ and $\eta = 1.18$ (η denotes noise type). The minimum mean square error for these values is $K = 15$ which is equal to the number of pure members. According to the graph, the power of the image error is decreasing, and the power of the noise error is increasing, and both are functions of the subspace dimensionality. Given the mentioned findings, 15 subspaces are extracted from the actual hyperspectral Indiana image, and the proposed algorithm is applied to them. Also Fig. 7 shows the evaluation of the mean square error for the HYSIME algorithm in University of Pavia as a function of the subspace dimensionality with $P = 8$ and SNR $= 50$ dB, for $\eta = 0$ and $\eta = 1.18$. The minimum mean square error for these values is $K = 8$ which is equal to the number of pure members. According to the graph, the power of the image error is decreasing, and the power of the noise error is increasing, and both are functions of the subspace dimensionality.

Table 1 Hyperspectral subspace estimated using HYSIME for white noise and Gaussian noise in Indian Pines image

SNR	P							
	η=0				$\eta = \frac{1}{18}$			
50	3	5	10	15	3	5	10	15
35	3	5	10	15	3	5	10	15
25	3	5	10	14	3	5	10	11
15	3	5	8	9	3	5	8	8

Table 2 Hyperspectral subspace estimated using HYSIME for white noise and Gaussian noise in Salinas image

SNR	P							
	η=0				$\eta = \frac{1}{18}$			
50	3	5	10	15	3	5	10	15
35	3	5	10	14	3	5	10	11
25	3	5	10	12	3	5	10	12
15	3	5	9	8	3	5	6	8

Table 3 Hyperspectral subspace estimated using HYSIME for white noise and Gaussian noise in University of Pavia image

SNR	P							
	η=0				$\eta = \frac{1}{18}$			
50	2	4	6	8	2	4	6	8
35	2	4	6	8	2	4	6	7
25	2	4	6	8	2	4	6	7
15	2	4	5	6	2	4	3	6

Given the mentioned findings, 8 subspaces are extracted from the actual hyperspectral Pavia image, and the proposed algorithm is applied to them. After dimensionality reduction with the help of the HYSIME method, edge-preserving filtering (EPF), and classifying the hyperspectral subspaces using a support vector machine (SVM), the results obtained from the classification have been presented. These results were then merged into the decision-making level using majority rule to create the spectral-spatial classifier. Tables 4–6 show the number of training samples. For each of the three hyperspectral data, 30 samples are considered. Training samples were randomly selected from the ground truth data.

It is worth noting that based on previous research, we set $\sigma_s = 7$, 4 for the Indian Pines and the University of Pavia, respectively[22]. Also, the best range σ_r for the three sets of data is between 0.1 and 0.3[22]. For the Salinas image, the best classification function in the proposed method is $\sigma_s = 5$. Figs. 2–4 shows the implementation results and the classification maps obtained from the Indian Pines, Salinas and University of Pavia hyperspectral images in the proposed method dependent on the corresponding OA criterion. For categorization based on spatial information, the proposed method of HYSIME-EPF-SVM is used for low space. The logic behind the success is to estimate hyperspectral subcomponents for combining results for subspace using the HYSIME technique. In this case, we can increase classification performance without allocating spectral information. The results in Tables 4–6 show that HYSIME-EPF-SVM in all cases provides better classification results than random subgroups and SVMs. The proposed HYSIME-EPF-SVM approach significantly improves the classification. Results using spectral information (HYSIME) indicate the im-

portance of EPF in extracting spatial information. The results shown in Tables 4–6 show that HYSIME-EPF-SVM is superior to RS-ICA-RGF-RF, PCA-PF-SVM and EPF-SVM, which has the efficacy of the combination of HYSIME and EPF shown through a group strategy. According to Figs. 2 and 3, in which the spectral-spatial

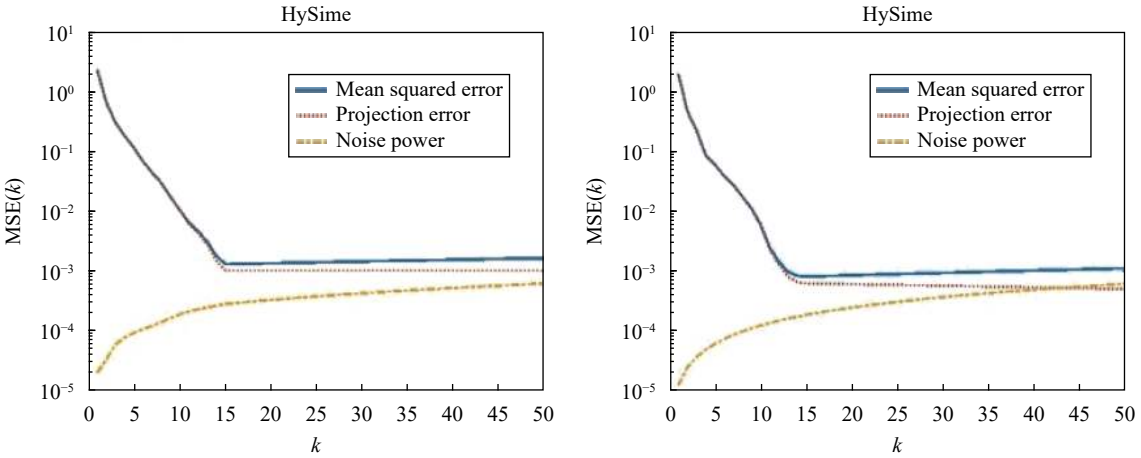

(a) Gaussian noise (b) White noise

Fig. 5 Plot of mean square error for (Indian Pines) hyperspectral data obtained by the HYSIME method

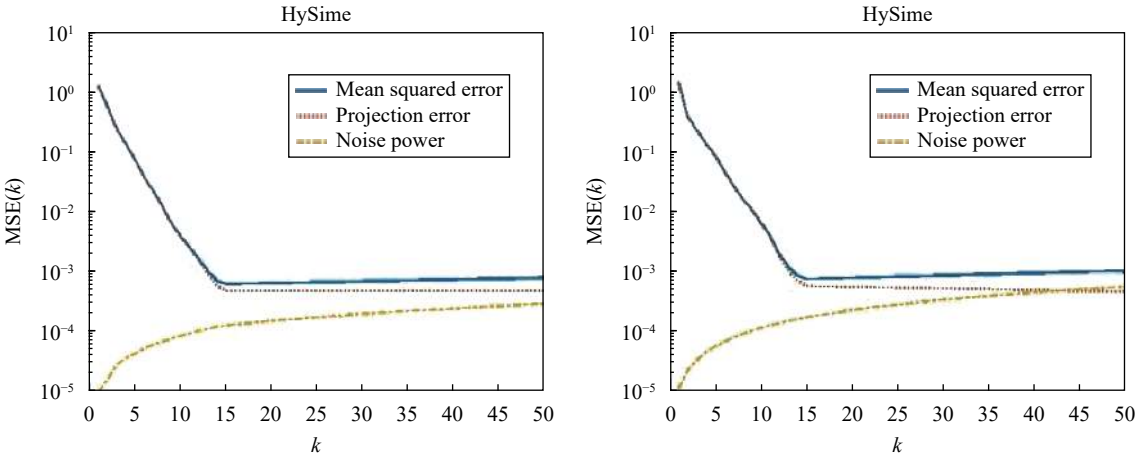

(a) Gaussian noise (b) White noise

Fig. 6 Plot of mean square error for (Salinas) hyperspectral data obtained by the HYSIME method

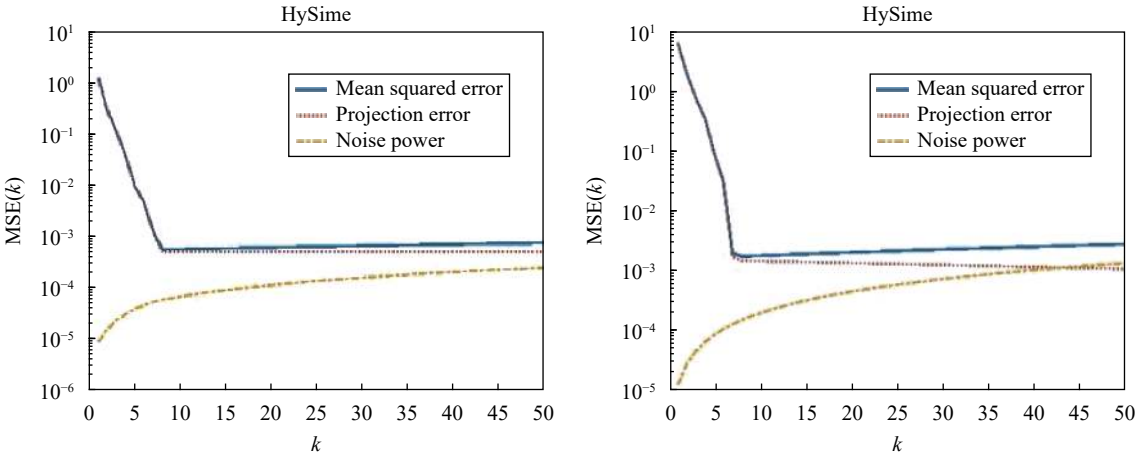

(a) Gaussian noise (b) White noise

Fig. 7 Plot of mean square error for (University of Pavia) hyperspectral data obtained by the HYSIME method

Table 4 Results of each class for Indian Pines hyperspectral data in the proposed method

	Indian Pines class	Train	Test	SVM	EPF-SVM[8]	PCA-PF-SVM[21]	RS-ICA-EPF-RF[11]	Proposed method	
								RS-EPF-SVM	HYSIME-EPF-SVM
1	Alfalfa	15	26	68.80	57.78	54.55	98.75	99.17	100
2	Corn-no till	30	1408	71.26	85.80	95.22	90.70	91.97	97.11
3	Corn-no till	30	810	73.91	89.35	94.97	89.47	93.38	97.65
4	Corn	30	217	62.28	43.06	91.44	99.75	99.26	97.82
5	Grass/Pasture	30	463	88.30	92.93	72.16	93.53	95.27	96.38
6	Grass/Trees	30	710	86.44	91.93	100	98.84	98.08	100
7	Grass/Pasture-mowed	15	14	88.07	82.35	81.92	99.23	98.46	100
8	Hay-windrowed	30	485	90.89	100	100	99.80	99.63	100
9	Oats	15	10	77.77	100	54.45	100	100	100
10	Soybeans-no till	30	952	74.42	66.32	84.34	91.86	88.40	93.35
11	Soybeans-min till	30	2435	77.79	92.13	95.90	88.24	98.60	99.02
12	Soybean-clean	30	537	69.31	52.77	88.51	94.67	92.43	97.80
13	Wheat	30	185	91.84	100	95.85	99.34	99.23	99.60
14	Woods	30	1245	92.60	96.94	100	98.27	99.40	99.98
15	Building-Grass-Trees-Drives	30	366	68.84	88.99	72.58	98.23	85.10	97.56
16	Stone-steel Towers	30	73	99.05	87.95	87.01	99.08	92.20	97.15
	OA	–	–	79.53	83.03	91.54	93.15	93.43	98.79
	AA	–	–	80.01	83.02	81.06	96.23	96.56	98.32
	Kappa	–	–	77.0	81.02	90.01	–	94.86	99.0

Table 5 Results of each class for University of Pavia hyperspectral data in the proposed method

	Universityof Pavia class	Train	Test	SVM	EPF-SVM[8]	PCA-PF-SVM[21]	PCA-PFEPF-RF[11]	Proposed method	
								RS-EPF-SVM	HYSIME-EPF-SVM
1	Asphalt	30	6832	96.82	98.05	92.30	95.81	92.92	99.19
2	Meadows	30	18666	97.50	97.40	99.47	95.64	97.72	99.90
3	Gravel	30	2187	77.18	89.16	84.96	99.22	87.60	98.03
4	Trees	30	3416	87.90	96.20	76.68	96.68	97.78	89.75
5	Metal sheets	30	1358	97.38	95.05	99.92	93.24	99.68	99.92
6	Bare soil	30	5084	77.75	64.27	84.80	94.45	95.54	97.49
7	Bitumen	30	1336	67.5	58.20	85.61	90.88	92.08	99.77
8	Bricks	30	3858	85.91	76.20	79.43	92.75	92.18	99.31
9	Shadows	30	1006	99.91	99.89	96.95	96.41	99.96	88.91
	OA	–	–	90.57	87.00	90.41	94.54	95.83	98.88
	AA	–	–	87.22	86.05	88.90	95.01	95.37	99.09
	Kappa	–	–	88.0	83.03	89.02	–	95.79	98.31

classification results in Indian Pines and Salinas hyperspectral data are shown, the noise level in the classification map of the HYSIM-EPF-SVM proposed method is lower than the SVM method. Also, OA in the proposed method is more than the SVM method, so the HYSIME-EPF-SVM method leads to improved classification performance and increased classification accuracy. In Fig. 7, the spectral-spatial classification results from University of Pavia hyperspectral data is shown. The noise level in the classification map of the HYSIM-EPF-SVM proposed method is lower than the SVM method, also OA in the proposed method is more than SVM method, so the HYSIME-EPF-SVM method leads to improved classification performance and increased classification accuracy.

Table 6 Results of each class for Salinas hyperspectral data in the proposed method

	Salinas class	Train	Test	SVM	EPF-SVM[8]	PCA-PF-SVM[21]	Proposed method	
							RS-EPF-SVM	HYSIME-EPF-SVM
1	Weeds_1	30	1989	99.9	100	100	99.09	100
2	Weeds_2	30	3703	99.6	99.89	99.84	99.06	100
3	Fallow	30	1956	95.7	94.91	100	95.07	100
4	Fallow plow	30	1374	97.5	97.86	91.79	97.05	97.6
5	Fallow smooth	30	2658	98.3	99.96	99.52	98.03	99.3
6	Stubble	30	3939	100	99.92	99.97	100	98.62
7	Celery	30	3559	99.0	100	100	99.0	98.74
8	Grapes	30	11251	81.9	82.04	95.28	81.09	97.4
9	Soil	30	6183	99.5	99.48	99.97	99.5	99.8
10	Corn	30	3258	87.3	85.06	97.76	87.3	96.7
11	Lettuce 4wk	30	1048	96.6	98.21	100	96.6	97.65
12	Lettuce 5wk	30	1907	96.9	100	100	96.9	100
13	Lettuce 6wk	30	890	96.9	96.10	98.33	96.06	98.15
14	Lettuce 7wk	30	1052	89.2	99.20	93.09	89.02	99.8
15	Vinyard untrained	30	7248	64.2	73.97	85.01	64.2	86.4
16	Vinyard trellis	30	1787	95.0	99.49	95.21	95.0	100
	OA			89.21	91.41	96.11	94.65	97.31
	AA			93.59	95.38	97.24	97.44	97.24
	Kappa			88.01	90.03	96.01	94.04	96.78

The reason for choosing these images is the similarity of the spectral signature of different classes and therefor, the complexity of the classification may be increased. If the edge-preserving filtering is applied on the hyperspectral image without any selection of subspaces or random selection, the important information may be ignored. Our proposed method can extract the mentioned information and maintain the specific classes with the small objects.

Using edge preservation filtering (EPF) and HYSIME techniques ensures the neighboring that are of the same class have the same features, so it will reduce the changes in the areas belonging to one class for this reason, the HYSIME-EPF-SVM method has shown a significantly better performance than other methods. According to the Tables 4–6, using the proposed method, the average accuracy in these images in order is 98.79%, 97.31% and 98.88%, and the kappa coefficient will be capable of increasing significantly.

In order to explain the effect of the strategy for the subspace selection, we compare our results (HYSIME-EPF-SVM) with the random subspace approach that so-called RS-EPF-SVM. Figs. 2–4 (cases (c) and (d)) and Tables 4–6 show this comparison. For example, in Indian Pines, the OA is 93.43% and 98.79% for the RS-EPF-SVM and HYSIME-EPF-SVM methods, respectively. Furthermore, for the complexity of computing, we report the CPU time of both approaches in Table 7. Due to the random selection of subspace in RS-EPF-SVM method needs no extra process, it is easy to see that the time consuming of RS-EPF-SVM is less than HYSIME-EPF-SVM. However, the efficiency of HYSIME-EPF-SVM method from the point of view of accuracy is outperformed.

Table 7 Comparison of the CPU time for RS-EPF-SVM and HYSIME-EPF-SVM methods based on second

Dataset	RS-EPF-SVM method	HYSIME-EPF-SVM method
Indian Pines	76.87 s	105.11 s
University of Pavia	86.64 s	112.52 s
Salinas	77.55 s	109.51 s

4.4 Comparisons with other state-of-the classifier

We offer a comparison of the proposed methods against spectra-spatial classification, including EPF-SVM[8], PCA-PF-SVM[20] and ICA-EPF-RF[11] taking into account the number of training samples (i.e., 30 samples per three images). From Tables 4–6, we find that the proposed methods are better in terms of classification differentiation than these methods and are more stable than other spectral-spatial classifications. Details are given on the methods mentioned in the introduction.

5 Conclusions

In this paper, a new method based on automatic selection signal subspace using the HYSIME method and combining it with the spatial-spectral filtering of the EPF is proposed. In the algorithm, a subset of the eigenvectors with minimum mean square error selects the best representation of the signal subspace by estimating the signal and noise correlation matrix. So, HYSIME is an automatic method that does not need to adjust its parameters. The proposed method is superior to other methods for detecting the hyperspectral subspace. The results show the effectiveness of the proposed methods in extracting spectral and spatial features and providing higher classification accuracies when compared with state-of-the-art methods. In future work, we will utilize, other data sources in the classification process. As a suggestion, this algorithm can be compared with virtualized dimension algorithms such as Harsanyi-Farrand-Chang (HFC) and noise-whitened HFC (NWHFC).

References

[1] H. Liu, G. F. Xiao, Y. L. Tao, C. J. Ouyang. Multi-source remote sensing image registration based on contourlet transform and multiple feature fusion. *International Journal of Automation and Computing*, vol. 16, no. 5, pp. 575–588, 2019.

[2] D. Chutia, D. K. Bhattacharyya, K. K. Sarma, R. Kalita, S. Sudhakar. Hyperspectral remote sensing classifications: A perspective survey. *Transactions in GIS*, vol. 20, no. 4, pp. 463–490, 2016. DOI: 10.1111/tgis.12164.

[3] R. K. Pina, R. C. Puetter. Bayesian image reconstruction: The pixon and optimal image modeling. *Publications of the Astronomical Society of the Pacific*, vol. 105, no. 688, pp. 630–637, 1993. DOI: 10.1086/133207.

[4] L. Velásquez, J. P. Cruz-Tirado, R. Siche, R. Quevedo. An application based on the decision tree to classify the marbling of beef by hyperspectral imaging. *Meat Science*, vol. 133, pp. 43–50, 2017. DOI: 10.1016/j.meatsci.2017.06.002.

[5] E. Merényi, W. H. Farrand, J. V. Taranik, T. B. Minor. Classification of hyperspectral imagery with neural networks: Comparison to conventional tools. *EURASIP Journal on Advances in Signal Processing*, vol. 2014, no. 1, Article number 71, 2014. DOI: 10.1186/1687-6180-2014-71.

[6] M. Fauvel, J. Chanussot, J. A. Benediktsson. A spatial-spectral kernel-based approach for the classification of remote-sensing images. *Pattern Recognition*, vol. 45, no. 1, pp. 381–392, 2012. DOI: 10.1016/j.patcog.2011.03.035.

[7] G. Mountrakis, J. Im, C. Ogole. Support vector machines in remote sensing: A review. *ISPRS Journal of Photogrammetry and Remote Sensing*, vol. 66, no. 3, pp. 247–259, 2011. DOI: 10.1016/j.isprsjprs.2010.11.001.

[8] X. D. Kang, S. T. Li, J. A. Benediktsson. Spectral-spatial hyperspectral image classification with edge-preserving filtering. *IEEE Transactions on Geoscience and Remote Sensing*, vol. 52, no. 5, pp. 2666–2677, 2014. DOI: 10.1109/TGRS.2013.2264508.

[9] A. L. Li, A. Y. Qin, Z. W. Shang, Y. Y. Tang. Spectral-spatial sparse subspace clustering based on three-dimensional edge-preserving filtering for hyperspectral image. *International Journal of Pattern Recognition and Artificial Intelligence*, vol. 33, no. 3, Article number 1955003, 2019. DOI: 10.1142/S0218001419550036.

[10] B. Tu, X. F. Zhang, J. P. Wang, G. Y. Zhang, X. F. Ou. Spectral-spatial hyperspectral image classification via non-local means filtering feature extraction. *Sensing and Imaging*, vol. 19, no. 1, Article number 11, 2018. DOI: 10.1007/s11220-018-0196-9.

[11] J. S. Xia, L. Bombrun, T. Adalı, Y. Berthoumieu, C. Germain. Spectral-spatial classification of hyperspectral images using ICA and edge-preserving filter via an ensemble strategy. *IEEE Transactions on Geoscience and Remote Sensing*, vol. 54, no. 8, pp. 4971–4982, 2016. DOI: 10.1109/TGRS.2016.2553842.

[12] T. Zhang, N. Ai, L. Wang, J. Wang, J. Y. Peng. Spectral-spatial hyperspectral image classification based on sparse representation and edge preserving filtering. In *Proceedings of International Conference on the Frontiers and Advances in Data Science*, IEEE, Xi′an, China, pp. 165–170, 2017. DOI: 10.1109/FADS.2017.8253220.

[13] B. G. Cui, X. D. Ma, X. Y. Xie, G. B. Ren, Y. Ma. Classification of visible and infrared hyperspectral images based on image segmentation and edge-preserving filtering. *Infrared Physics & Technology*, vol. 81, pp. 79–88, 2017. DOI: 10.1016/j.infrared.2016.12.010.

[14] X. D. Kang, X. L. Xiang, S. T. Li, J. A. Benediktsson. PCA-based edge-preserving features for hyperspectral image classification. *IEEE Transactions on Geoscience and Remote Sensing*, vol. 55, no. 12, pp. 7140–7151, 2017. DOI: 10.1109/TGRS.2017.2743102.

[15] S. T. Li, K. Z. Zhang, Q. B. Hao, P. H. Duan, X. D. Kang. Hyperspectral anomaly detection with multiscale attribute and edge-preserving filters. *IEEE Geoscience and Remote Sensing Letters*, vol. 15, no. 10, pp. 1605–1609, 2018. DOI: 10.1109/LGRS.2018.2853705.

[16] S. W. Zhong, C. I. Chang, Y. Zhang. Iterative edge preserving filtering approach to hyperspectral image classification. *IEEE Geoscience and Remote Sensing Letters*, vol. 16, no. 1, pp. 90–94, 2019. DOI: 10.1109/LGRS.2018.2868841.

[17] H. Ghassemian. A review of remote sensing image fusion methods. *Information Fusion*, vol. 32, pp. 75–89, 2016. DOI: 10.1016/j.inffus.2016.03.003.

[18] L. Y. Fang, N. J. He, S. T. Li, A. J. Plaza, J. Plaza. A new spatial-spectral feature extraction method for hyperspectral images using local covariance matrix representation. *IEEE Transactions on Geoscience and Remote Sensing*, vol. 56, no. 6, pp. 3534–3546, 2018. DOI: 10.1109/TGRS.2018.2801387.

[19] T. X. Zhang, J. Y. Su, C. J. Liu, W. H. Chen. Potential bands of sentinel-2A satellite for classification problems in precision agriculture. *International Journal of Automa-*

tion and Computing, vol. 16, no. 1, pp. 16–26, 2019. DOI: 10.1007/s11633-018-1143-x.

[20] Q. Zhang, X. Y. Shen, L. Xu, J. Y. Jia. Rolling guidance filter. In *Proceedings of the 13th European Conference on Computer Vision*, Springer, Zurich, Switzerland, pp. 815–830, 2014. DOI: 10.1007/978-3-319-10578-9_53.

[21] Z. K. Chen, J. J. Jiang, X. W. Jiang, X. P. Fang, Z. H. Cai. Spectral-spatial feature extraction of hyperspectral images based on propagation filter. *Sensors*, vol. 18, no. 6, Article number 1978, 2018. DOI: 10.3390/s18061978.

[22] J. H. Rick Chang, Y. C. Frank Wang. Propagated image filtering. In *Proceedings of IEEE Conference on Computer Vision and Pattern Recognition*, IEEE, Boston, USA, pp. 10–18, 2015. DOI: 10.1109/CVPR.2015.7298595.

[23] J. M. Bioucas-Dias, J. M. P. Nascimento. Hyperspectral subspace identification. *IEEE Transactions on Geoscience and Remote Sensing*, vol. 46, no. 8, pp. 2435–2445, 2008. DOI: 10.1109/TGRS.2008.918089.

[24] X. Wu, B. Huang, L. Z. Wang, J. Q. Zhang. GPU-based parallel design of the hyperspectral signal subspace identification by minimum error (HySime). *IEEE Journal of Selected Topics in Applied Earth Observations and Remote Sensing*, vol. 9, no. 9, pp. 4400–4406, 2016. DOI: 10.1109/JSTARS.2016.2574876.

[25] B. T. Zhang, X. P. Wang, Y. Shen, T. Lei. Dual-modal Physiological Feature Fusion-based Sleep Recognition Using CFS and RF Algorithm methods. *International Journal of Automation and Computing*, vol. 16, no. 3, pp. 286–296, 2019. DOI: 10.1007/s11633-019-1171-1.

[26] P. Jain, V. Tyagi. A survey of edge-preserving image denoising methods. *Information Systems Frontiers*, vol. 18, no. 1, pp. 159–170, 2016. DOI: 10.1007/s10796-014-9527-0.

Negin Alborzi received the B. Eng. degree in computer engineering from Ayandegan Institute of Higher Education in Tonekabon, Iran in 2016. She is currently a Master student in information technology at Department of Computer Engineering Faculty of Electrical and Computer Engineering, Ayandegan Institute of Higher Education in Tonekabon, Iran.

Her research interest is data mining.

E-mail: Negginalborzi@gmail.com

ORCID iD: 0000-0003-2472-1307

Fereshteh Poorahangaryan received the B. Eng. degree in electronics engineering from Amirkabir University, Iran in 2006, and the M. Eng. degree in electronics engineering from Guilan University, Iran in 2009. She received the Ph. D. degree in electronics engineering from the Science and Research Branch of Islamic Azad University, Iran in 2017.

Her research interests include image processing, computer vision, and medical image analysis.

E-mail: f.ahangaryan@gmail.com (Corresponding author)

ORCID iD: 0000-0003-4947-1965

Homayoun Beheshti received the B. Eng. degree in computer engineering from North University, Iran in 2004, and the M. Eng. degree in network engineering from Sharif University of Technology, Iran in 2010. He is currently a Ph. D. degree candidate at Islamic Azad University, Iran.

His research interests include natural language processing (NLP) and data mining.

E-mail: Homayoun.Beheshti@gmail.com